AIMS Materials Science, 3(3): 927-937.
DOI: 10.3934/matersci.2016.3.927
Received: 24 May 2016
Accepted: 15 July 2016
Published: 18 July 2016

http://www.aimspress.com/journal/Materials

Research article

Effect of ZnO nanoparticles on the power conversion efficiency of organic photovoltaic devices synthesized with CuO nanoparticles

Aruna P. Wanninayake, Benjamin C. Church, and Nidal Abu-Zahra*

Materials Science and Engineering Department, University of Wisconsin-Milwaukee, 3200 North Cramer Street, Milwaukee, WI 53201, USA

* **Correspondence:** Email: nidal@uwm.edu; Tel: 414-229-2668.

Abstract: Polymer solar cells were fabricated with varying amounts of electron transporting ZnO NPs in a buffer layer located over an active layer of P3HT/PCBM incorporating a fixed amount of CuO nanoparticles. The enhanced electronic and optical properties attained by adding ZnO nanoparticles proportionally increased the power conversion efficiency by 32.19% compared to a reference cell without ZnO-NPs buffer layer. ZnO-NPs buffer layer improved the exciton dissociation rate, electron mobility, optical absorption and charge collection at the anode, resulting in higher short circuit current and external quantum efficiency. The short circuit current (J_{sc}) of the optimum device was measured at 7.620 mA/cm^2 compared to 6.480 mA/cm^2 in the reference cell with 0.6 mg of CuO nanoparticles. Meanwhile, the external quantum efficiency (EQE) increased from 54.6% to 61.8%, showing an enhancement of 13.18% with the incorporation of ZnO nanoparticle layer.

Keywords: ZnO nanoparticles; CuO nanoparticles; EQE; UV-visible spectroscopy; PSCs

1. Introduction

Bulk heterojunction polymer solar cells (PSCs), which are based on interpenetrating network of conjugated polymer donor and fullerene derivative acceptor materials, have attracted much attention in recent years due to their advantages of easy fabrication, simple device structure, low cost, light weight, and capability to be fabricated into flexible devices [1,2]. In recent times, many different

organic donor materials have been investigated [3,4,5] while electron acceptors remain the bottleneck in these studies. The power conversion efficiency (PCE) of PSCs with [6, 6]-phenyl-C61-butyric acid methyl ester (PCBM) electron acceptors has reached up to 9%. However, there are some critical drawbacks with complex processing methods and oxidation of the acceptors in ambient conditions [6,7]. Considering their stability under ambient conditions and high electron mobility, inorganic nanomaterials such as ZnO, CdSe and TiO_2 are among the most suitable electron acceptors to incorporate with the polymer donor in hybrid solar cells [8,9,10]. Among these nanomaterials ZnO, a low temperature crystalline material, is one of the most promising electron acceptors for solar cells.

Several studies were conducted to understand the role of ZnO as an electron transport layer embedded in PSCs. Sekine et al. [11] reported 4% PCE with 25% improvement for PSCs with ZnO electron accepting layer while Oh et al. [12] reported 3.39% PCE for ZnO nanoparticles (NPs) doped poly (3-hexylthiophene)/ [6, 6]-phenyl-C61-butyric acid methyl ester/ (P3HT/PCBM) PSCs. P3HT/PCBM devices with ZnO nanoparticles, as an electron transporting layer, exhibited an improved power conversion efficiencies up to 3.26% [13]. Zhu et al. [14] obtained a 3.5% maximum PCE for PSCs with 15 nm diameter ZnO NPs incorporated in a buffer layer. Gao et al. [15] improved the PCE of PSCs from 3.03% to 3.84% via hydrogen treatment of ZnO electron transport layers. Iwan et al. [16] reported 1.2% of PCE for the ZnO buffer layer embedded organic solar cells grown by Atomic Layer Deposition (ALD) method.

In a previously reported work [17], CuO NPs were successfully incorporated in the P3HT/PCBM active layer as a donor candidate. The combined effect of the P3HT and CuO NPs enhanced the optical absorption and exciton generation rate leading to better donor properties in the active layer. CuO is a p-type semiconductor with a band gap energy of 1.5 eV, which is close to the ideal energy gap of 1.4 eV [18], and ZnO is an n-type semiconductor which has a wide band gap energy of 3.37 eV. Kidowaki et al. revealed the suitability of CuO/ZnO hetero-structure for solar cells [19,20,21].

This study demonstrates the enhancement of power conversion efficiency of PSCs containing CuO NPs incorporated in P3HT/ PC70BM film with a ZnO-NPs buffer layer. The combined effect of CuO and ZnO-NPs was studied by UV-visible analysis, current voltage (J-V) characteristics, atomic force microscopy, and EQE measurements. In addition, the electrical performance of the hybrid solar devices is presented in this work.

2. Materials and Methods

2.1. Materials

Glass substrates measuring 24 × 80 × 1.2 mm (12 Ω/cm^2) with an ITO conductive layer of 25–100 nm were purchased from nanocs.com. PEDOT/PSS mixed in distilled water (Viscosity 14 cP) was obtained from Sigma Aldrich and it was mixed with an equal amount of distilled water. Active layer materials, P3HT and PC70BM were purchased from Rieke Metals and SES Research; respectively. Nanoparticles of ZnO (18nm diameter) and CuO (35 nm to 50 nm diameter) were purchased from nanocs.com. Aluminium coils with a diameter of 0.15 mm were purchased from Ted-Pella, Inc. (tedpella.com). All processing and characterization work of the PSC devices were conducted under same experimental conditions.

2.2. Solar Cells Fabrication

The conductive glass substrates were ultrasonically cleaned with ammonium hydroxide, hydrogen peroxide, distilled water, methyl alcohol, and isopropyl alcohol; successively. The fabrication of polymer based solar cells containing zinc oxide and copper oxide NPs was done in a N_2 filled glove box. The P3HT-PC70BM blend was obtained by mixture (1:1 ratio in weight) of regioregular P3HT and PC70BM (10 mg each) with 2ml of chlorobenzene (C_6H_5Cl) and mixing for 14 hours at 60 ^oC. CuO NPs were dispersed in 2 ml of C_6H_5Cl and were added to the mixture, so that the weight ratios of P3HT/PCBM/CuO-NPs in the final blend was 10:10:0.6 mg. Different amounts of ZnO nanoparticles were dispersed in pure ethanol to make four solutions with concentrations of 10, 20, 30, and 40 mg ml^{-1} of NPs.

The structure of the fabricated solar cell devices is schematically presented in Figure 1(a). The solar cell devices were spun coated in a glove box with N_2 atmosphere. A 40 nm-thick PEDOT/PSS layer, which serves as a thin hole-transport layer, was spun coated at a rotational velocity of 4000 rpm, followed by heating at 120 °C for 20 minutes in air. When the temperature of the samples reached the ambient temperature, the blends with P3HT:PC70BM: CuO NPs and ZnO solution were spun coated for two minutes at 1000 rpm and 2000 rpm; respectively. In this study, five different devices (reference cell, 10, 20, 30 and 40 mg ml^{-1} ZnO NPs in the buffer layer) were fabricated. These samples are denoted as A, B, C, D and E; respectively. The active layers measured 120 nm in average thickness and 0.12 cm^2 in surface area. The ZnO film thickness obtained was approximately 60 nm. The upper cathode layer with a thickness of approximately 100nm was formed by thermally evaporating Aluminum under high vacuum.

2.3. Solar Cells Characterization

The current density-voltage (J-V) characterization was carried out for all PSCs using a UV solar simulator with an AM 1.5G filter and a lamp intensity of 100 mW/cm^2. A source meter (Keithley 2400) was used to obtain the J-V measurements. Device parameters such as short circuit current (J_{sc}), open circuit voltage (V_{oc}), fill factor (FF) and power conversion efficiency (PCE) were recorded under ambient conditions. A quantum efficiency measurement kit (Newport-425) embedded in the solar cell simulator was used to obtain EQE values. A PerkinElmer LAMBDA 650 spectrophotometer, was used to obtain the optical properties of cells containing varying amounts of ZnO NPs. Agilent 5420 atomic force microscope (AFM) was used to analyze the surface morphology of the devices. Pico Image Basics and Gwyddion software were used to determine the root mean square surface roughness (σ_{rms}).

3. Results and Discussion

The architecture of the energy levels of hybrid solar cell devices is schematically shown in Figure 1b [19,22]. The highest occupied molecular orbital (HOMO) and lowest unoccupied molecular orbital (LUMO) energy bands of P3HT are formed at −5.2 eV and −3.53 eV; respectively. Similarly, in the PCBM molecules, the HOMO and LUMO levels are formed at −6.3 eV and −3.9 eV; respectively [23]. The conduction band (CB) of the ZnO NPs aligns at −4.1 eV while the LUMO level of the PEDOT: PSS forms at −5.0 eV [24]. The energy difference between valence band (VB)

and conduction band (CB) of the CuO NPs is found to be 2.07eV [18]. Hence, the P3HT combined with CuO NPs forms a strong donor phase, which can produce more excitons (electron-hole pairs) into the structure. These donor materials and PC70BM acceptor molecules create a donor-acceptor (D/A) heterojunction, which can dissociate the excitons generated in the donor structure [25].

The energy gradient lowest unoccupied molecular orbital (LUMO) of P3HT (−3.5 eV) and the conduction band edge (−4.1 eV) of ZnO is close to 1.1 eV resulting in a better exciton dissociation through fast electron injection to ZnO layer. Similarly, the arrangement of the energy levels of CuO and ZnO forms D/A pairs for rapid electrons transfer from CuO NPs to ZnO NPs. This rapid electron transfer will also help to dissociate the excitons. The ZnO NPs create a high potential barrier for holes in the P3HT to travel to the ZnO buffer layer. With a small forward bias stimulation, the electrons are moved to conduction bands (CB) of P3HT and CuO, and transferred to the LUMO of PC70BM acceptor materials as well as ZnO NPs. Whereas, holes move from the donor to the ITO anode. If holes move to the ZnO layer, electrons and holes can be recombined generating leakage current, which leads to lower power conversion efficiency. However, ZnO buffer layer provides an energy barrier to prevent hole penetration into the valence band (VB) of ZnO.

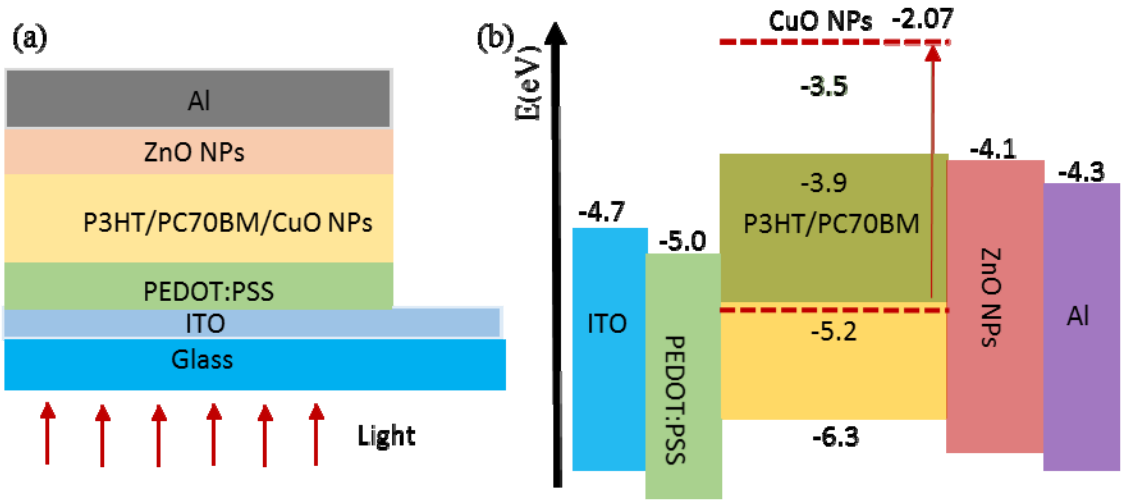

Figure 1. Graphical representation of the hybrid device architecture (a) Layer structure with ZnO buffer layer, (b) energy level diagram.

The surface morphology of the active layers was studied by AFM as shown in Figure 2. AFM images show that the assembly of an electron transporting ZnO NPs layer on the active layer increases the roughness of the P3HT/PC70BM/CuO-NPs films. The measured root-mean-square roughness (σ_{rms}) value of the P3HT/PC70BM/CuO layer was 0.33 nm and after depositing the ZnO NPs layer on the active layer, the σ_{rms} value increased to 0.89 nm. Sample E (P3HT/PCBM/CuO-0.6 mg NPs with 40 mg of ZnO NPs) exhibited a maximum surface roughness of 0.97 nm. These roughened surfaces provide better interfacial contact with the Al layer and hence enhance the charge collection ability at the Al cathode. Also, enhanced roughness can result in greater light absorption due to the diffuse reflection between the active layer and the cathode. In the ZnO NPs layers, the electrons mobility (6.6×10^{-2} cm^2 V^{-1} s^{-1}) [26] is remarkably higher than that (1.7×10^{-4} cm^2 V^{-1} s^{-1}) [27] of the amorphous TiO_x thin film. Hence, ZnO NP layer can act as an effective electron transporting medium.

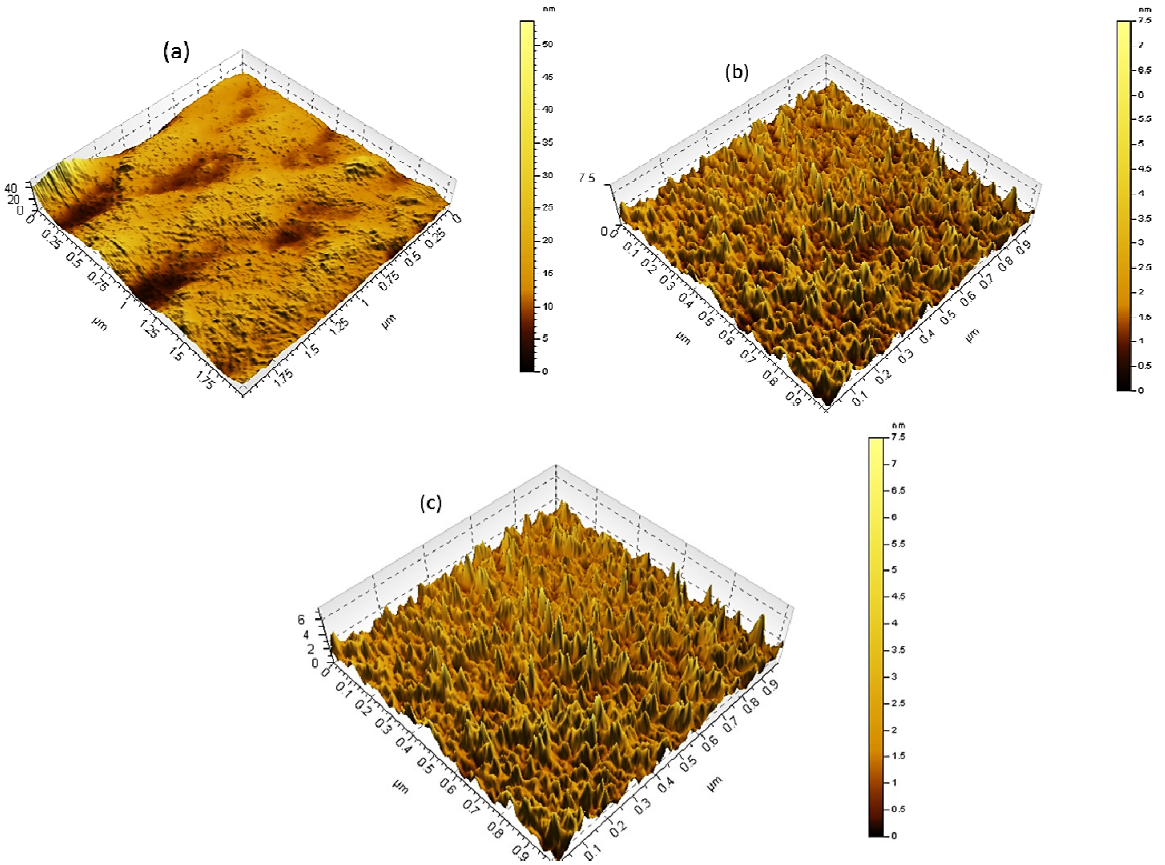

Figure 2. AFM images of active layer (2 × 2 μm^2 scans) with (a) P3HT/PCBM/CuO-0.6 mg NPs (sample A), (b) P3HT/PCBM/CuO-0.6 mg NPs with 20 mg of ZnO NPs buffer layer (sample C), and (c) P3HT/PCBM/CuO-0.6 mg NPs with 40mg of ZnO NPs buffer layer (sample E).

The UV−visible absorption spectra of the P3HT/PC70BM, P3HT/PC70BM/CuO, and P3HT/PC70BM/CuO/ZnO, are comparatively shown in Figure 3. The wavelength range of these absorption spectra is between 350 nm and 550 nm. The absorption intensities of the fabricated devices exhibited enhancements over the entire range. The optical absorption peak intensity of the P3HT/PC70BM thin layer is 0.31 and after incorporating CuO NPs in the blend, absorption intensity was improved to 0.63. Meanwhile, the ZnO NPs buffer layer assembled P3HT/PC70BM/ CuO NPs increased the absorption intensity to 0.76. Therefore, the CuO NPs and ZnO NPs led to higher optical absorption in the solar cells over the entire wavelength range.

A higher optical absorption yields more electrons-holes generation, higher carrier mobility, and more carrier injection to the electrodes resulting in better power conversion efficiency of the solar device. As mentioned earlier, the roughness values of P3HT/PC70BM/ CuO assembled with a ZnO NPs buffer layer were improved and this rougher surface can reflect more light between the ZnO layer and the Al cathode. In addition, an increase in the surface area, due to higher surface roughness, enhances the absorption spectra of the P3HT/PC70BM/CuO and ZnO NPs compared to the P3HT/PCBM reference film [28].

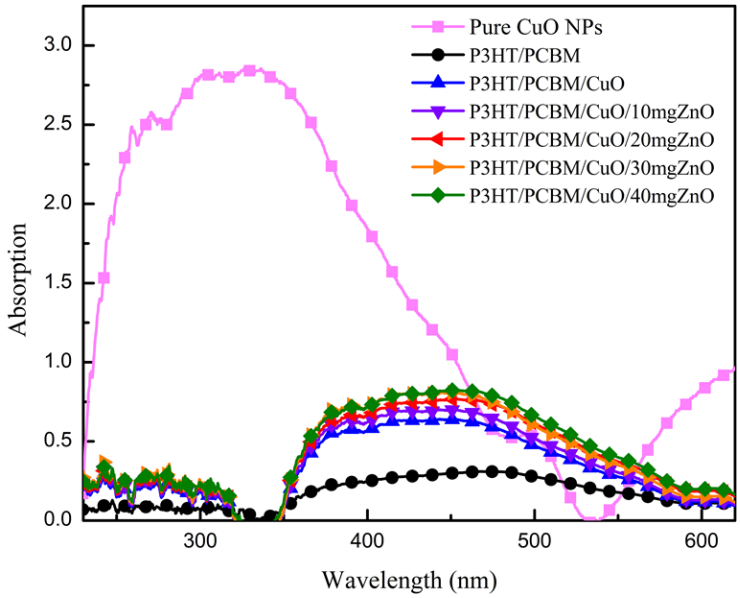

Figure 3. Optical absorption spectra of the hybrid solar cells with CuO and ZnO NPs.

The EQE or the incident photon to current conversion efficiencies (IPCE) measurements describe the ratio between the incident photons on the solar cell, from the input source, and the generated free charges carriers by the solar cell. The enhanced light absorption, exciton dissociation rate, carrier collection at the electrodes and improved charge carrier mobility strongly affect the EQE measurements. Figure 4 shows the corresponding EQE measurements. When the particle densities in the ZnO buffer layer were increased, relevant EQEs were proportionally increased in the wavelength range from 310 nm to 650 nm. The peak values of the EQE for samples A, B, C, D, and E are 54.6%, 56.8%, 61.8%, 60% and 57.7%; respectively.

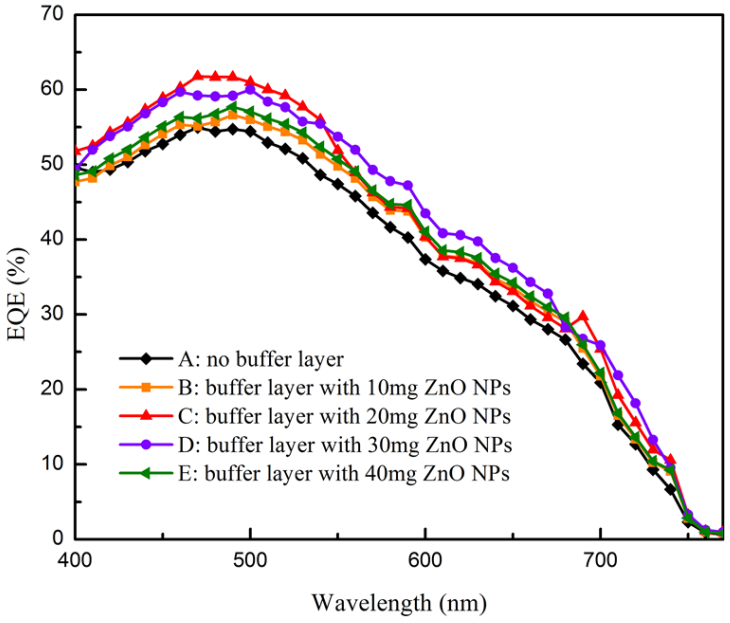

Figure 4. EQE of the hybrid solar cells with ZnO buffer layer.

CuO NPs incorporated P3HT/PCBM blends provide two main electron-transporting paths: a conventional path through the PCBM molecules and hopping sites created by CuO NPs. The CuO NPs produce dense PCBM clusters with hopping sites creating an efficient electron flow towards the ZnO electron transport layer. The enhancement of EQE measurements within the wavelength range of UV absorption spectra is generally attributed to PCBM molecules. The EQE spectra within the wavelength range between 350 nm and 550 nm, shown in Figure 4, provide evidence for such measurements. The ZnO electron transport buffer layer provides extremely high electron transporting facility to the Al electrodes uplifting the EQE profile. Therefore, the separated free electrons from excitons, created in P3HT and CuO NPs phases, can be transported through interconnected PCBM domains and CuO NPs hopping centers towards the ZnO buffer layer. ZnO structure gives high momentum to the electrons towards the cathode. As a result, the electron mobility is remarkably enhanced with high EQE.

The EQE has a linear relationship with the J_{sc} of the solar cell devices. The J_{sc} is the major determinant of power conversion efficiency; where PCE = $(J_{sc}*V_{oc}*FF)/P_{in}$. The J_{sc} values obtained for each cell followed a similar trend to EQE, which shows that the cells with 0.06 mg of ZnO NPs in the electron transport buffer layer exhibit the highest J_{sc} values. Table 1 summarizes the photovoltaic performance parameters, such as J_{sc}, V_{oc}, fill factor (FF), and PCE, for all the fabricated devices. The corresponding current−voltage (J-V) characteristics with AM 1.5G irradiation (100 mW cm^{-2}) of solar cells using different ZnO NPs electron transporting buffer layers are shown in Figure 5.

Table 1. Electric parameters of ITO/PEDOT:PSS P3HT/PCBM/CuO-0.6 mg NPs/ZnO NPs/ Al solar cells.

Sample	J_{sc}(mA/cm^2)	V_{oc}(V)	FF(%)	Rs (Ω/cm^2)	R_{sh} (Ω/cm^2)	PCE(%)
A	6.480±0.01	0.677±0.004	68.11±0.03	9.2±0.01	152±2	2.988±0.007
B	7.063±0.03	0.688±0.003	71.44±0.01	8.4±0.11	165±5	3.472±0.016
C	7.620±0.07	0.696±0.007	74.47±0.06	7.8±0.04	190±7	3.950±0.044
D	7.437±0.01	0.702±0.008	72.46±0.02	8.0±0.02	149±4	3.784±0.032
E	7.379±0.05	0.714±0.012	69.79±0.08	8.3±0.05	123±1	3.677±0.10
P3HT/PCBM + ZnO buffer layer (No CuO NPs)	5.513±0.06	0.696±0.004	66.14±0.11	8.8±0.04	168±5	2.538±0.017

As shown in table 1, the control device without ZnO electron transporting buffer layer shows J_{sc} of 6.48 mA cm^{-2}, FF of 68.11%, V_{oc} of 0.677 V and a power conversion efficiency (PCE) of 2.988%. However, PCE clearly increased after assembling the ZnO electron transport layer next to the P3HT/PC70BM/CuO layer. The optimum photovoltaic parameters were obtained by the devices with 20 mg ZnO NPs (sample C) in the electron transport layer, which exhibit a J_{sc} of 7.620 mA cm^{-2}, a FF of 74.47%, a V_{oc} of 0.696 V and a PCE of 3.950%.

However, as the ZnO NPs content increased further, the PCE of the solar cells decreased. The PCE of the device with 40mg of ZnO in the buffer layer decreased by 6.9%, and the photovoltaic parameters also decreased correspondingly to J_{sc} of 7.379 mA cm^{-2} and a reduced FF of 69.79%, leading to a final PCE of 3.68%. The fill factor (FF) mainly depends on the structural morphology of the active layer and the series resistance of the devices [29,30]. However, the fill factor decreased from 74.47% to 69.79% with increasing the amount of ZnO in the buffer layer. The series resistance of the device increases with increasing the amount of ZnO NPs in the electron transport buffer layer (Table 1). This may be the main reason that J_{sc} and FF tend to decrease beyond the optimum amount of ZnO NPs in the samples. Furthermore, increase of ZnO NPs in the buffer layer, exceeding the optimum amount of 20 mg, allows the ZnO NPs to penetrate to P3HT/PCBM/CuO film and changing nanoscale morphology within P3HT/PCBM /CuO blend. This morphology change causes a significant reduction of donor/acceptor contact surface, thus lowering the EQE and J_{sc} of the cells.

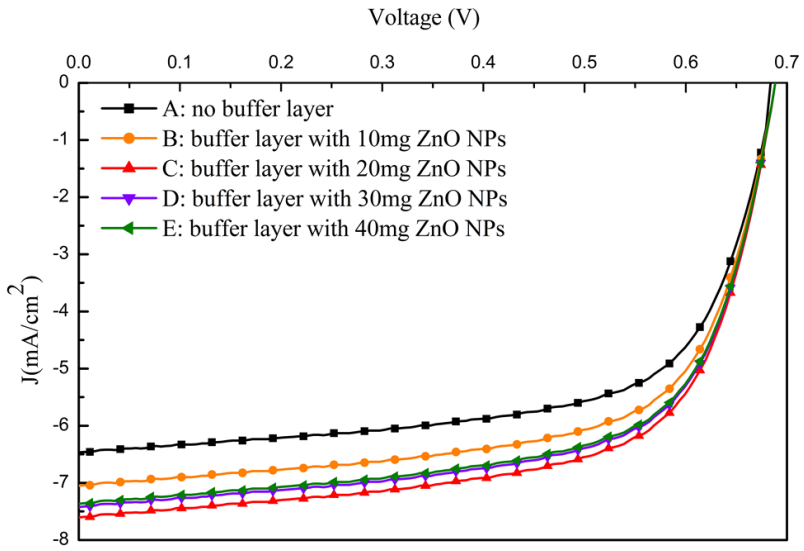

Figure 5. *J-V* characteristics of hybrid polymer solar cells ZnO buffer layer.

Open circuit voltage (V_{oc}) has a linear relationship to the energized band levels within D-A phases. The V_{oc} of a hybrid solar cell can be increased by moving the polymer HOMO level further away from the vacuum level [31]. However, V_{oc} did not change significantly, possibly since the LUMOs of P3HT and PC70BM were constant; thus suggesting that the reduced recombination due to increased carrier mobility did not improve V_{oc}. On the other hand, the HOMO energy level of P3HT in the active layer was not influenced by the ZnO buffer layer in the solar cell device. Therefore; ZnO-NPs did not enhance V_{oc} in the solar cells [32].

4. Conclusion

In this study, ZnO nanoparticles are incorporated in an electron transport buffer layer assembled on top of the P3HT/PC70BM/CuO NPs active later. After incorporating the electron transport layer, the PCE increased from 2.988% to 3.950% in the cells containing 20 mg ZnO-NPs (sample C) in the buffer layer, which is equivalent to a 32.19% improvement in efficiency. The higher performance is

attributed to enhanced EQE, electron mobility, exciton dissociation and optical absorption due to CuO and ZnO NPs in the device. The optical absorption spectrum exhibited significant improvement in the presence of ZnO-NPs buffer layer due to the elevated exciton generation rate. AFM analysis show an increase in surface roughness of the active layer after depositing the ZnO nanoparticles incorporated electron transport buffer layer, which results in a larger contact area between ZnO and the Al cathode.

Conflict of Interest

All authors declare no conflicts of interest in this paper.

References

1. Dang MT, Hirsch L, Wantz G (2011) Best Seller in Polymer Photovoltaic Research. *Adv Mater* 23: 3597–3602.
2. Wang PH, Lee HF, Huang YC, et al. (2014) The Proton Dissociation Constant of Additive Effect on Self-Assembly of Poly(3-hexyl-thiophene) for Organic Solar Cells, Electron. *Mater Lett* 10: 767–773.
3. Zhang F, Mammo W, Andersson LM, et al. (2006) Low-Bandgap Alternating Fluorene Copolymer/Methanofullerene Heterojunctions in Efficient Near-Infrared Polymer Solar Cells. *Adv Mater* 18: 2169–2173.
4. Huang Y, Guo X, Liu F, et al. (2012) Improving the Ordering and Photovoltaic Properties by Extending–Conjugated Area of Electron-Donating Units in Polymers with D-A Structure. *Adv Mater* 24: 3383–3389.
5. Wang E, Tao L, Wang Z, et al. (2010) An Easily Synthesized Blue Polymer for High-Performance Polymer Solar Cells. *Adv Mater* 22: 5240–5244.
6. Reese M.O., Nardes A.M., Rupert B.L., et al. (2010) Photoinduced Degradation of Polymer and Polymer–Fullerene Active Layers: Experiment and Theory. *Adv Funct Mater* 20: 3476–3483.
7. He Z, Mei Z, Su S, et al. (2012) Enhanced power-conversion efficiency in polymer solar cells using an inverted device structure. *Nature Photon* 6: 591–595.
8. Shao S, Liu J, Zhang B, et al. (2011) Enhanced stability of zinc oxide-based hybrid polymer solar cells by manipulating ultraviolet light distribution in the active layer. *Appl Phys Lett* 98: 203304–203307.
9. Huang J, Yin Z, Zheng Q (2011) Applications of ZnO in organic and hybrid solar cells. *Energy Environ Sci* 4: 3861–3877.
10. Lin Y-Y, Chu T-H, Li S-S, et al. (2009) Interfacial Nanostructuring on the Performance of Polymer/TiO2 Nanorod Bulk Heterojunction Solar Cells. *J Am Chem Soc* 131: 3644–3649.
11. Sekine N, Chou CH, Kwan WL, et al. (2009) ZnO nano-ridge structure and its application in inverted polymer solar cell. *Org Electron* 10: 1473–1477.
12. Oh SA, Heo SJ, Yang JS, et al. (2013) Effects of ZnO Nanoparticles on P3HT:PCBM Organic Solar Cells with DMF-Modulated PEDOT:PSS Buffer Layers. *ACS Appl Mater Interfaces* 5: 11530–11534.

13. Wu Z, Song T, Xia Z, et al. (2013) Enhanced performance of polymer solar cell with ZnO nanoparticle electron transporting layer passivated by in situ cross-linked three-dimensional polymer network. *Nanotechnology* 24: 484012.
14. Zhu F, Chen X, Lu Z, et al. (2014) Efficiency Enhancement of Inverted Polymer Solar Cells Using Ionic Liquid-functionalized Carbon Nanoparticles-modified ZnO as Electron Selective Layer. *Nano-Micro Lett* 6: 24–29.
15. Gao HL, Zhang XG, Meng JH, et al. (2015) Enhanced efficiency in polymer solar cells via hydrogen plasma treatment of ZnO electron transport layers. *J Mater Chem A* 3: 3719–3725.
16. Iwan A, Palewicz M, Tazbir I, et al. (2016) Influence of ZnO:Al, MoO_3 and PEDOT:PSS on efficiency in standard and inverted polymer solar cells based on polyazomethine and poly(3-hexylthiophene). *Electrochimica Acta* 191: 784–794.
17. Wanninayake A, Gunashekar S, Li S, et al. (2015) Performance enhancement of polymer solar cells using copper oxide nanoparticles. *Semicond Sci Technol* 30: 064004.
18. Wanninayake AP, Gunashekar S, Li S, et al. (2015) CuO Nanoparticles Based Bulk Heterojunction Solar Cells: Investigations on Morphology and Performance. *J Sol Energy Eng* 137: 031016.
19. Kidowaki H, Oku T, Akiyama T (2012) Fabrication and characterization of CuO/ZnO solar cells. *J Phys Conf Ser* 352: 012022.
20. Ikram M, Murrayc R, Imran M, et al. (2016) Enhanced performance of P3HT/ (PCBM: ZnO: TiO2) blend based hybrid organic solar cells. *Mater Res Bull* 75: 35–40.
21. Ikram M, Murray R, Hussain A, et al. (2014) Hybrid organic solar cells using both ZnO and PCBM as electron acceptor materials. *Mater Sci Eng B* 189: 64–69.
22. Qian L, Yang J, Zhou R, et al. (2011) Hybrid polymer-CdSe solar cells with a ZnO nanoparticle buffer layer for improved efficiency and lifetime. *J Mater Chem* 21: 3814–3817.
23. Wang M, Wang X (2008) P3HT-ZnO bulk-heterojunction solar cell sensitized by a perylene derivative. *Sol Energy Mater Sol Cells* 92: 766–771.
24. Beek WJE, Wienk MM, Janssen RAJ (2006) Hybrid Solar Cells from Regioregular Polythiophene and ZnO Nanoparticles. Adv Funct Mater 16: 1112–1116.
25. Ochiai S, Kumar P, Santhakumar K, et al. (2013) Examining the Effect of Additives and Thicknesses of Hole Transport Layer for Efficient Organic Solar Cell Devices. *Electron Mater Lett* 9: 399–403.
26. Kim JY, Kim SH, Lee HH, et al. (2006) New Architecture for High-Efficiency Polymer Photovoltaic Cells Using Solution-Based Titanium Oxide as an Optical Spacer. *Adv Mater* 18: 572–576.
27. Roest L, Kelly JJ, Vanmaekelbergh D, et al. (2002) Staircase in the Electron Mobility of a ZnO Quantum Dot Assembly due to Shell Filling. *Phys Rev Lett* 89: 036801.
28. Ikram M, Ali S, Murray R, et al. (2015) Influence of fullerene derivative replacement with TiO_2nanoparticles in organic bulk heterojunction solar cells. *Curr Appl Phys* 15: 48–54.
29. Djara V, Bernède J (2005) Effect of the interface morphology on the fill factor of plastic solar cells. *Thin Solid Films* 493: 273–277.
30. Oo T, Mathews N, Tam T, et al. (2010) Investigation of photophysical, morphological and photovoltaic behavior of poly (p-phenylene vinylene) based polymer/oligomer blends. *Thin Solid Films* 518: 5292–5299.

31. Ji CH, Oh IS, Oh SY (2015) Improving the performance of organic solar cells using an electron transport layer of B4PyMPM self-assembled nanostructures. *Electron Mater Lett* 11: 795–800.
32. Shahini A, Abbasian K (2012) Charge carriers and excitons transport in an organic solar cell-theory and simulation. *Electron Mater Lett* 8: 435–443.

AIMS Press